ABSTRACT

PERFORMANCE EVALUATION OF SUBCARRIER MAPPING TECHNIQUES FOR MULTIUSER IN PRESENCE OF DOPPLER IN LTE UPLINK

Kushal Kumar Ponugoti, M.S.
Department of Electrical Engineering
Northern Illinois University, 2014
Dr. Mansour Tahernezhadi, Director

Orthogonal frequency division multiplexing (OFDM) is an advanced 3G/4G scheme which achieves high data rate and combats multipath fading. However, OFDM systems suffer from nonlinear peak to average power ratio (PAPR) and carrier frequency offsets (CFO). These two factors lead to degraded performance and thereby reducing the system efficiency. In order to reduce the PAPR, the single carrier frequency division multiple access (SCFDMA) in the long-term evolution (LTE) uplink was developed. In this thesis, the bit error rate (BER) and PAPR for localized frequency division multiple access (LFDMA), modified hybrid frequency division multiple access (MHFDMA) and zero interleaved frequency division multiple access (IFDMA) in the presence of multipath fading and Doppler have been evaluated and compared. The MHFDMA has been designed using the LFDMA and IFDMA subcarrier mapping techniques in SCFDMA. The multiuser SCFDMA system is simulated using different number of subcarriers and modulation schemes. In terms of PAPR, IFDMA gives a lower value compared to the MHFDMA and LFDMA but its implementation is complex for the base station. The LFDMA gives a higher PAPR value compared to the IFDMA and MHFDMA, but it gives a lower value compared to the conventional OFDM systems. The implementation complexity of LFDMA is very low. The MHFDMA gives a PAPR in between LFDMA and IFDMA with the

implementation complexity also in between LFDMA and IFDMA. However, it extracts the multiuser diversity and frequency diversity of both the schemes. The system is simulated for four users and 1024 subcarriers, with each user accessing 256 subcarriers, in the presence of Doppler and multipath Rayleigh fading channel. The BER performance for all the three subcarrier mapping techniques was the same in no Doppler case and different percentage Doppler cases. The BER performance degraded as the constellation size in the modulation increased.

NORTHERN ILLINOIS UNIVERSITY

DEKALB, ILLINOIS

DECEMBER 2014

PERFORMANCE EVALUATION OF SUBCARRIER MAPPING TECHNIQUES FOR MULTIUSER IN PRESENCE OF DOPPLER IN LTE UPLINK

BY

KUSHAL KUMAR PONUGOTI

A THESIS SUBMITTED TO THE GRADUATE SCHOOL

IN PARTIAL FULFILLMENT OF THE REQUIREMENTS

FOR THE DEGREE

MASTER OF SCIENCE

DEPARTMENT OF ELECTRICAL ENGINEERING

Thesis Director:

Dr. Mansour Tahernezhadi

TABLE OF CONTENTS

Page

Page

LIST OF TABLES

Page

LIST OF FIGURES

Page

Page

CHAPTER 1: INTRODUCTION

1.1 Background

Wireless communication has been one of the major areas of focus since the late 20th century. The demand for large bandwidth and high communication speed is growing at a rapid pace. Due to the increased demand in mobile applications, next-generation wireless mobile system is designed in such a way that they not only support voice call but also provide high-performance data applications over radio-wave communication system [1]. In order to satisfy these demands, wireless technologies like GSM, OFDM, UWB, LTE, XLTE and LTE-A came into existence.

3G mobile communication systems were modeled using the code division multiple access (CDMA) scheme. OFDM technology is the basis for 4G wireless communication systems. 4G wireless technologies like LTE, LTE-A and worldwide interoperability for microwave access (WiMAX) operate in the 2-4 GHz frequency region and provide data rates of 100-200 Mbps. Communication takes place in two ways: uplink and downlink. Verma and Sharma [2] state that "the uplink represents the transmission from a mobile terminal to base station, and downlink represents the transmission from a base station to mobile terminal" (p. 2207). With a wider transmission bandwidth, the signal bandwidth becomes greater than the coherence bandwidth leading to inter-symbol interference (ISI) caused by frequency selectivity of the wireless channel which becomes more serious in a single-carrier communication system [3]. One way to counter effects of frequency selectivity is to use a multicarrier technique which divides the total channel bandwidth into smaller bandwidth portions [3]. OFDM satisfies this requirement as it is a

multicarrier system. However, OFDM system has its own disadvantages. It suffers from high PAPR and also has very high sensitivity to CFO. In order to overcome this issue, the Third-Generation Partnership Project (3GPP) introduced the SCFDMA system in the physical layer of LTE uplink [4].

1.2 Problem Statement

OFDM signal is the superposition of all the individual signals placed on each subcarrier. The superposition leads to a high peak value compared to the average signal value. This leads to a high PAPR value. PAPR value increases as the number of subcarriers increases, and it does not depend on the modulation scheme used. Presence of high peak power signals in the transmitter requires high-power semiconductor amplifiers with large operating region. Designing and implementing such power amplifiers is very costly and also leads to performance degradation. Large peak values force the power amplifiers to go into the saturation region where the signal gets clipped. In this region, the orthogonal nature of the subcarriers is lost which leads to inter-carrier interference (ICI). The situation is even worse when Doppler combined with multipath propagation is present in the system.

To overcome the effect of high PAPR in the uplink, SCFDMA technique is employed. The subcarrier mapping module in the SCFDMA helps to overcome the high PAPR issue. OFDM is a multicarrier modulation technique, where data is transmitted on multiple carriers. SCFDMA is a single-carrier modulation technique where data is transmitted on a single carrier. The difference between OFDM and SCFDMA system is the presence of DFT (discrete Fourier transform) and subcarrier mapping block in the transmitter and the corresponding IDFT (inverse discrete Fourier transform) and subcarrier demapping block in the receiver. In localized mode, the M-pt DFT

outputs are mapped onto subcarriers which are continually spaced in the channel bandwidth [4, 5]. In interleaved mapping, the DFT outputs of the input data are mapped onto subcarriers which occupy the whole channel bandwidth [5]. In both mapping schemes, the unused subcarriers are zeroes [4, 6]. In this thesis, a modified hybrid technique is developed from the existing hybrid technique developed by F.S. Al-kamali [4], using the localized and interleaved modes. BER performance for LFDMA, IFDMA and MHFDMA for multiple users is compared in the presence of Doppler and multipath propagation.

1.3 Thesis Structure

This thesis is framed as follows:

- In Chapter 2, multipath propagation and Doppler effect are studied. The wireless channel characteristics are explained in detail and modeled.
- Chapter 3 deals with the advantages of multicarrier over single-carrier modulation techniques. OFDM system is explained in detail, listing the advantages and drawbacks.
- Chapter 4 explains about the PAPR problem in OFDM systems. The SCFDMA system is introduced and compared with the OFDM technique.
- In Chapter 5, the two existing subcarrier mapping techniques (LFDMA and IFDMA) and the hybrid schemes are explained, and the modified hybrid technique is explained, which is a combination of IFDMA and LFDMA.

- Chapter 6 contains the simulation parameters for the three mapping techniques mentioned in Chapter 5, and the results of BER in the presence of Doppler are compared.
- In Chapter 7, the thesis is concluded, and possible future work is suggested.

CHAPTER 2: WIRELESS CHANNEL MODELLING

2.1 Multipath Propagation

In wireless communication systems, different copies (of the same signal) come to the receiver at different times and with different attenuations. These copies add up at the receiver either constructively or destructively, which leads to either constructive or destructive interference. Multipath occurs due to reflections from buildings, mountains, water bodies, etc. In wireless communications, air is the medium or channel of propagation. Multipath propagation causes errors and hence it degrades the performance of communication. The transmitted signal is represented as x(t), received signal as y(t) and the channel as h(t). The relation between the three parameters is shown in Figure 2.1.

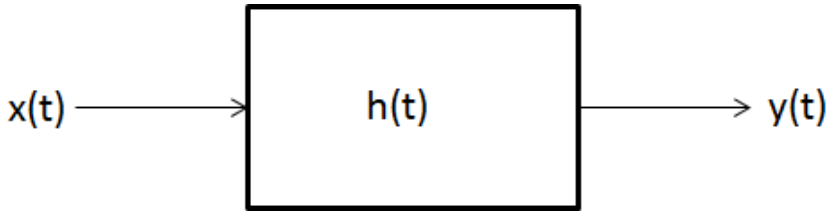

Figure 2.1: Relation Between x, h and y.

Consider a situation where the signal reaches to the receiver via a direct path and L multipath as demonstrated in Figure 2.2. Direct path is also known as line of sight (LOS). Indirect path is labeled as non-line of sight (NLOS). The impulse response of the channel can be modeled as shown in equation 2.1.

$$h(t) = a_0\delta(t-\tau_0) + a_1\delta(t-\tau_1) + a_2\delta(t-\tau_2) + \cdots + a_L\delta(t-\tau_L) \quad (2.1)$$

a_L and τ_L are the attenuation and delay associated with L^{th} path [7].

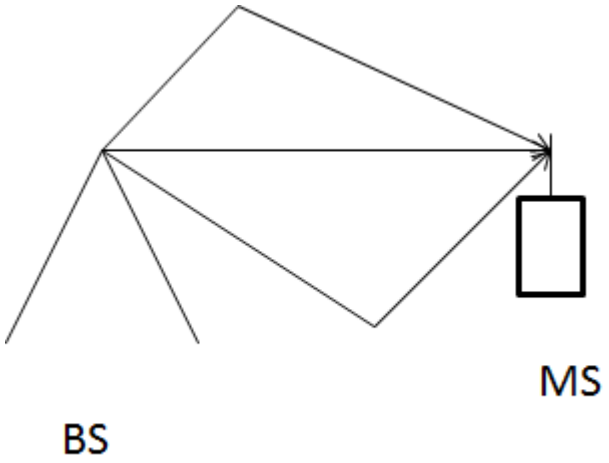

Figure 2.2: Multipath Communication.

Equation 2.1 can be further simplified as shown in equation 2.2.

$$h(t) = \sum_{i=0}^{L-1} a_i \delta(t - \tau_i) \tag{2.2}$$

The wireless signal S(t) whose carrier signal is f_c is given by equation 2.3.

$$S(t) = Re\{S_b(t) e^{j2\pi f_c t}\} \tag{2.3}$$

$S_b(t)$ is known as the complex baseband equivalent. The net signal obtained at the receiver combined with the multipath is given by equation 2.4.

$$y(t) = Re\{\sum_{i=0}^{L-1} (a_i S_b(t - \tau_i))$$

$$y_b(t) = \sum_{i=0}^{L-1} a_i S_b(t - \tau_i) \tag{2.4}$$

In practical applications, the value of τ_i is in the order of few microseconds (~1µs). A signal is said to be a narrow band signal if

$$f_m < \frac{1}{\tau_i} \tag{2.5}$$

For a narrow band signal $S_b(t-\tau_i) = S_b(t)$

$$y_b(t) = S_b(t)\sum_{i=0}^{L-1} a_i e^{-j2\pi f_c \tau_i} \tag{2.6}$$

According to the above equation 2.6, we receive a range of variable power signals at the receiver in practical applications [7]. This phenomenon wherein we achieve signals of variable power is known as fading. The fading coefficient 'h' is given by equation 2.7.

$$h = \sum_{i=0}^{L-1} a_i e^{-j2\pi f_c \tau_i} \tag{2.7}$$

2.2 Statistics of Fading Coefficient

The fading coefficient given by equation 2.7 can be split into two random variables. One random variable is real while the other is imaginary. It is shown in equations 2.8 and 2.9.

$$h = \sum_{i=0}^{L-1} a_i e^{-j2\pi f_c \tau_i} = X + jY = ae^{j\varphi} \tag{2.8}$$

$$h = \sum_{i=0}^{L-1} (a_i \cos(2\pi f_c \tau_i) - j a_i \sin(2\pi f_c \tau_i)) \tag{2.9}$$

Upon splitting these terms and assigning them to the two random variables, we get the following results:

$$X = \sum_{i=0}^{L-1} a_i cos2\pi f_c \tau_i \text{ and } Y = \sum_{i=0}^{L-1} a_i sin2\pi f_c \tau_i$$

The probability density function of the two random variables is given by equation 2.10 [7].

$$f_{A,\varphi} = \frac{1}{\pi} e^{-a^2} \det(J_{XY}) \tag{2.10}$$

J is called as the Jacobian matrix. Let us assume $x = a\cos\varphi; y = a\sin\varphi$:

$$x^2 + y^2 = a^2$$

$$J = \begin{bmatrix} \frac{\partial X}{\partial a} & \frac{\partial Y}{\partial a} \\ \frac{\partial X}{\partial \varphi} & \frac{\partial Y}{\partial \varphi} \end{bmatrix} = \begin{bmatrix} cos\varphi & sin\varphi \\ -asin\varphi & acos\varphi \end{bmatrix}$$

$$\therefore f_{A,\varphi} = \frac{a}{\pi} e^{-a^2} \tag{2.11}$$

The probability distribution function is given by equation 2.12 which is the marginal of the density function with respect to 'a' over a fixed interval.

$$f_A(a) = \int_{-\pi}^{\pi} f_{A,\varphi}(a,\varphi) d\varphi = \int_{-\pi}^{\pi} \frac{a}{\pi} e^{-a^2} d\varphi$$

$$f_A(a) = 2ae^{-a^2} \qquad 0 \leq a \leq \infty \tag{2.12}$$

Equation (2.1) represents the envelope of fading power. This is famously known as Rayleigh fading. It occurs due to the multipath propagation in the wireless channel. In this multipath environment the signal fades according to the Rayleigh distribution. A typical Rayleigh distribution is shown in Figure 2.3. From the Figure it is evident that signal power is very low in deep fading conditions. The received signal cannot be distinguished from noise when a deep fade occurs.

The probability density of 'a' and φ are given by equations 2.13 and 2.14.

$$2ae^{-a^2} \qquad 0 \leq a \leq \infty \tag{2.13}$$

$$\frac{1}{2\pi} \qquad -\pi \leq \varphi \leq \pi \tag{2.14}$$

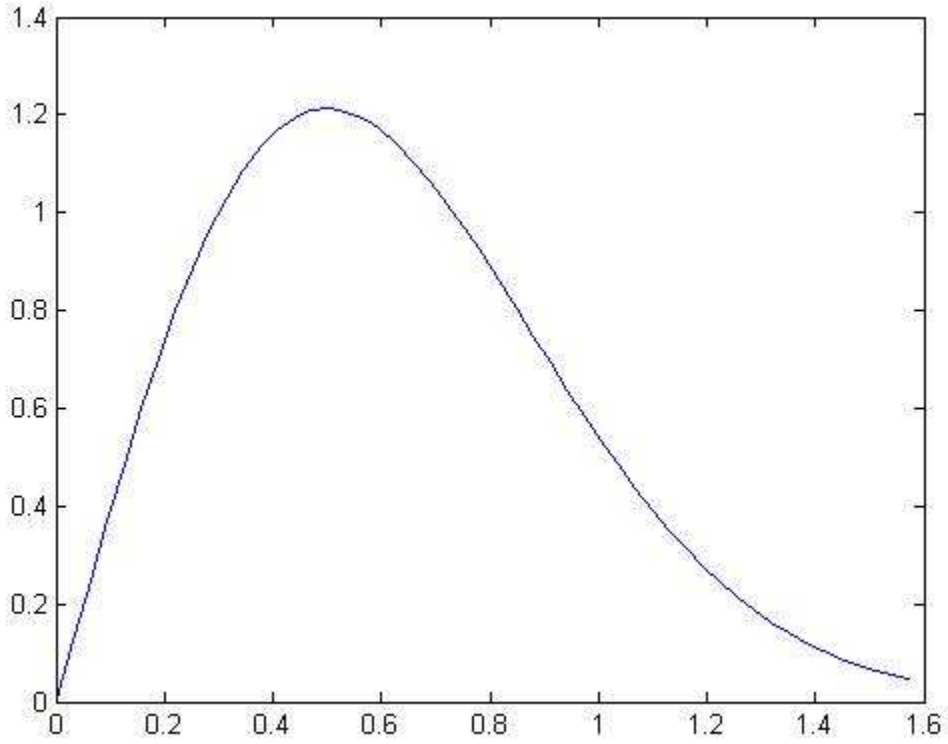

Figure 2.3: Rayleigh Distribution.

2.3 Delay Spread

Section 2.2 described about the fading coefficient. This section deals with the power profile characteristics and delay spread of the channel. A case of four multipath channels is considered where the gain and delay associated with each path is shown in Table 2.1.

Table 2.1: Gain and Delay Values

Gain (g)	Delay (τ)
$\|a_0\|^2$	τ_0
$\|a_1\|^2$	τ_1
$\|a_2\|^2$	τ_2
$\|a_3\|^2$	τ_3

Power profile of the channel is given by equation 2.15.

$$\varphi(\tau) = |h(\tau)|^2$$

$$= \sum_{i=0}^{L-1} a_i^2 \delta(\tau - \tau_i)$$

$$= \sum_{i=0}^{L-1} g_i \delta(\tau - \tau_i) \qquad (2.15)$$

Hence we get multiple copies due to scattering. These copies are occurring over an interval of time [8]. This time interval is termed “delay spread,” shown in Figure 2.4.

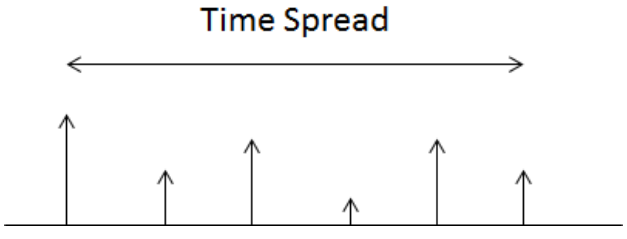

Figure 2.4: Delay Spread.

2.3.1 Maximum Delay Spread

The first component of the signal arrives after a delay of τ_0 and the last component comes to the receiver atτ_{L-1}. The maximum delay spread is given by equation 2.16.

$$\sigma_{\tau\max} = \tau_{L-1} - \tau_0 \tag{2.16}$$

2.3.2 RMS Delay Spread

Maximum delay spread is not the exact way to the spread as signals received after a long time will have very less power. These signals will not be detected by the receiver and hence taking small signal power values is not an efficient way to calculate the delay spread. An efficient way to get around the problem is by using root mean square (RMS) delay spread. In RMS delay spread, low power paths are not considered in calculating delay spread.

g_i is the power associated with the i^{th} multipath. Normalized fraction of power in the i^{th} path is given by equation 2.17.

$$b_i = \frac{g_i}{g_0 + g_1 + \cdots + g_{L-1}}$$

$$b_i = \frac{g_i}{\sum_{j=0}^{L-1} g_j} \tag{2.17}$$

Average delay is given by equation 2.18.

$$\tau' = b_0\tau_0 + b_1\tau_1 + \cdots + b_{L-1}\tau_{L-1}$$

$$\tau' = \sum_{i=0}^{L-1} b_i\tau_i$$

$$\tau' = \sum_{i=0}^{L-1} \frac{g_i\tau_i}{\sum_{j=0}^{L-1} g_j} = \frac{\text{weighted delay}}{\text{total power}} \tag{2.18}$$

Using the value of average delay, the RMS delay spread can be calculated.

$$\sigma_\tau^2 = b_0(\tau_0 - \tau')^2 + b_1(\tau_1 - \tau')^2 + \cdots + b_{L-1}(\tau_{L-1} - \tau')^2$$

$$= \sum_{i=0}^{L-1} b_i(\tau_i - \tau')^2$$

$$= \sum_{i=0}^{L-1} \frac{g_i(\tau_i - \tau')^2}{\sum_{i=0}^{L-1} g_i}$$

$$\sigma_\tau = \sqrt{\sum_{i=0}^{L-1} \frac{g_i(\tau_i - \tau')^2}{\sum_{j=0}^{L-1} g_j}} \tag{2.19}$$

2.4 Coherence Bandwidth

The coherence bandwidth can be calculated by taking the Fourier transform of the channel delay profile. Upon taking the Fourier transform, a low pass sort of characteristics is observed. The frequency band remains constant or flat for some portion of the characteristics. The flat portion is termed as coherence bandwidth. A typical spectrum is shown in Figure 2.5. Coherence bandwidth is abbreviated as B_c. If the shape of output spectrum of the transmitted signal is the same as the shape of the input spectrum, distortion is eliminated; i.e., if the bandwidth of the signal is less than or equal to the coherence bandwidth, distortion is combatted. Such a channel is known as a frequency nonselective or flat fading channel.

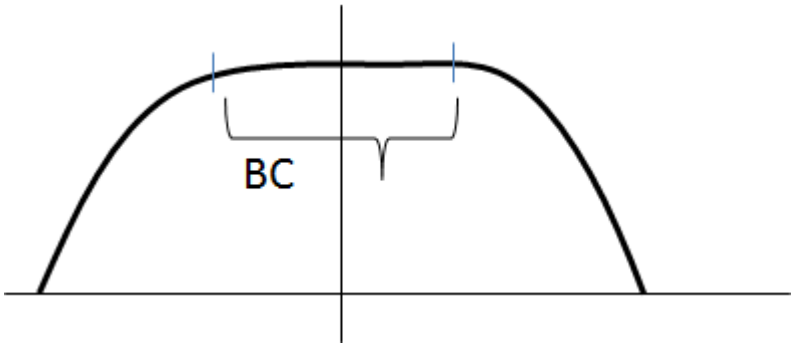

Figure 2.5: Coherence Bandwidth Spectrum.

If signal bandwidth is greater than the coherence bandwidth, the edges of input are attenuated due to which the output gets distorted. Such a phenomenon is known as frequency selective fading response. Equation 2.20 represents the Fourier transform of the channel.

$$H(f) = \sum a_i e^{-j2\pi f \tau_i} \tag{2.20}$$

Mathematically, coherence bandwidth in terms of delay spread is given by equation 2.21.

$$B_c = \frac{1}{2\sigma_\tau} \tag{2.21}$$

If the delay spread is less than the symbol duration, the same symbol is interfering with itself. If delay spread is larger than symbol duration, previous symbol interferes with the current symbol. This is known as ISI or inter-block interference (IBI) [8]. This is the main reason why GSM is a flat fading system while 3G/4G is a frequency selective fading system. Equalizers are used in 3G/4G systems to make the frequency response flat. ISI leads to loss of data at the receiver and hence degrades communication systems.

2.5 Doppler Shift

The phenomenon where there is a change in the frequency of the electromagnetic (EM) wave due to the relative motion between the transmitter and the receiver is known as the Doppler effect. This particular frequency change has to be countered in real-time communication systems as it produces erroneous results. Figure 2.6 shows the setup which achieves Doppler.

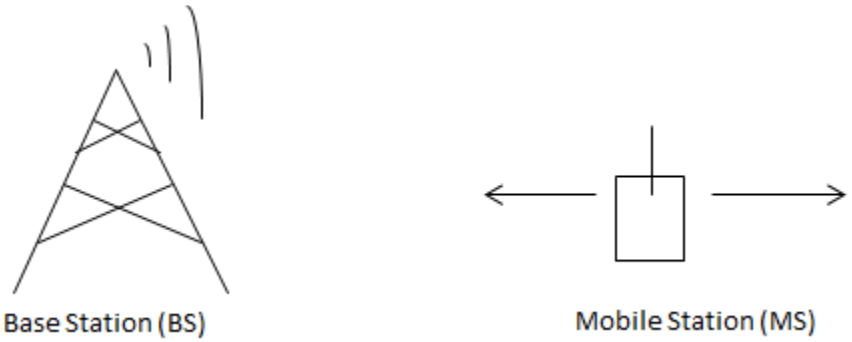

Figure 2.6: Cause of Doppler Effect.

2.5.1 Computation of Doppler Shift

Consider a situation where the MS is moving at an angle θ with respect to the BS as shown in Figure 2.7.

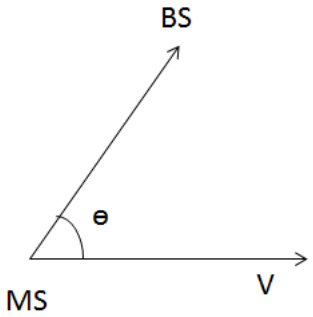

Figure 2.7: Motion of BS.

The received frequency f_r is now equal to the sum of carrier frequency f_c and the Doppler frequency f_d as shown in equation 2.22.

$$f_d = \frac{V cos\theta}{c} * f_c$$

$$f_r = f_c + f_d = f_c + \frac{V cos\theta}{c} * f_c \tag{2.22}$$

$0 \leq \theta \leq \frac{\pi}{2}$: The MS is moving towards the BS

$\frac{\pi}{2} \leq \theta \leq \pi$: The MS is moving away from the BS

For any other condition, even though the MS has a velocity, there is no effect of Doppler on the system whatsoever. For typical values of f_c = 1850 MHz, V = 60 mph towards BS, the computed Doppler shift is about 165 Hz. The received frequency is therefore 1850 MHz + 165 Hz. This value may look small, but it has a huge impact.

2.5.2 Effect on Channel

Let us represent the baseband channel as $a_i\delta(t - \tau_i)$. Here a_i represents the attenuation of i^{th} path and τ_i represents the delay of the i^{th} path. After time t, distance between the MS and the BS decreases by Vt. Hence the delay along this path also decreases by a factor $\tau_i - \frac{Vt}{c}$. If the MS is moving at an angle θ with respect to the base station, the delay becomes $\tau_i - \frac{V cos\theta t}{c}$. The flat fading channel coefficient h is given as

$$h = \sum_{i=0}^{L-1} a_i e^{-j2\pi f_c \tau_i}$$

The flat fading coefficient now changes because it is now a function of t. This is because the MS is in relative motion with the BS. The new flat fading coefficient is given by equation 2.23.

$$h(t) = \sum_{i=0}^{L-1} a_i \, e^{-j2\pi f_c \tau_i(t)} \tag{2.23}$$

Substituting the delay value from theoretical analysis we get equation 2.24.

$$h(t) = \sum_{i=0}^{L-1} a_i \, e^{-j2\pi f_c \left(\tau_i - \frac{V cos\theta t}{c}\right)} \tag{2.24}$$

Equation 2.24 can be split into two portions as follows:

$$h(t) = \sum_{i=0}^{L-1} a_i e^{-j2\pi f_c \tau_i} \; e^{j2\pi f_c \left(\frac{v cos\theta t}{c}\right)}$$

$$h(t) = \sum_{i=0}^{L-1} a_i e^{-j2\pi f_c \tau_i} \; e^{j2\pi f_d t} \tag{2.25}$$

The Doppler term present in equation 2.25 gives rise to a time varying phase. Hence Doppler has resulted in a time varying channel. This is also known as time selective channel. At this juncture we can define another parameter known as the coherence time T_c. Coherence time is the time over which the channel is approximately constant [8]. Mathematically coherence time is equal to the reciprocal of four times the maximum Doppler shift. In practical wireless applications the coherence time is about 1ms. So in order to get the knowledge about the channel we need to measure the channel once every coherence time [8]. This is the major implication of coherence time.

2.5.3 Doppler Spectrum

The Doppler spectrum gives an intuition into the rate of change of the wireless channel. In order to compute the Doppler spectrum, the correlation function of the channel is needed. Correlation is the measure of similarity or dissimilarity. Consider two random variables X and Y. If the correlation between X and Y is high, then X and Y are similar. Mathematically the correlation between two random variables X and Y is nothing but the expected value of the product of the random variables. It is mathematically represented as E{XY*}. Let the channel coefficient at time t is given by $a_i(t)$.

$$a_i(t) = a_i e^{-j2\pi f \tau_i} e^{j2\pi f_d t}$$

If $E\{a_i(t) * a_i^*(t + \Delta t)\}$ is high, then the channel hasn't changed.

$$a_i(t + \Delta t) = a_i e^{-j2\pi f \tau_i} e^{j2\pi f_d (t+\Delta t)}$$

$$\psi(\Delta t) = E\{|a_i|^2 e^{-j2\pi f_d \Delta t}\}$$

$$\psi(\Delta t) = E\{a_i(t + \Delta t)\}$$

Normalizing$|a_i|^2 = 1$, we get the equation 2.26.

$$\psi(\Delta t) = E\left\{e^{-j2\pi f_d \Delta t}\right\} \quad (2.26)$$

This is known as the correlation coefficient. Substituting the value of Doppler frequency we get

$$\psi(\Delta t) = E\left\{e^{-\frac{j2\pi f_c V}{c} cos\theta \Delta t}\right\} \quad (2.27)$$

We know that $f_{dmax} = \frac{f_c V}{c}$ $when\ \theta = 0$. Therefore the equation 2.27 becomes equation 2.28.

$$\psi(\Delta t) = E\left\{e^{-j2\pi f_{dmax} cos\theta \Delta t}\right\} \quad (2.28)$$

Assuming that θ is uniformly distributed between 0 and π, we get equation 2.29.

$$\psi(\Delta t) = \int_0^{\pi} \frac{1}{\pi} e^{-j2\pi f_{dmax}\Delta t cos\theta \, d\theta} \tag{2.29}$$

The solution for equation 2.29 is in terms of the Bessel function and it is as follows:

$$\psi(\Delta t) = J_0(2\pi f_{dmax}\Delta t)$$

Where J_0 is the Bessel function of 0^{th} order [8]. The above expression can also be written as

$$\psi(\Delta t) = J_0\left(\frac{2\pi\Delta t}{4T_c}\right) = J_0\left(\frac{\pi}{2} * \frac{\Delta t}{T_c}\right) \tag{2.30}$$

In practical applications, any correlation below 0.5 is considered as a change in channel parameters [8]. Finally the Doppler spectrum is nothing but the Fourier transform of the autocorrelation function [8], i.e., equation 2.30, which is given as follows;

$$S_H(f) = \int_{-\infty}^{\infty} \psi(\Delta t) e^{-j2\pi f\Delta t} \, d(\Delta t)$$

$$S_H(f) = \int_{-\infty}^{\infty} J_0(2\pi f_{dmax}\Delta t) e^{-j2\pi f\Delta t} \, d(\Delta t)$$

$$S_H(f) = \frac{\frac{1}{\pi f_{dmax}} rect\left(\frac{f}{f_d}\right)}{\sqrt{1 - \left(\frac{f}{f_d}\right)^2}} \tag{2.31}$$

Equation 2.31 represents the Doppler spectrum. The plot of the above spectrum is shown in Figure 2.8. It is evident from the plot that the Doppler spectrum exists only between the intervals $-f_d$ to f_d. The spectrum shown in Figure 2.8 is also known as U-shaped spectrum or Jake's spectrum or Jake's model.

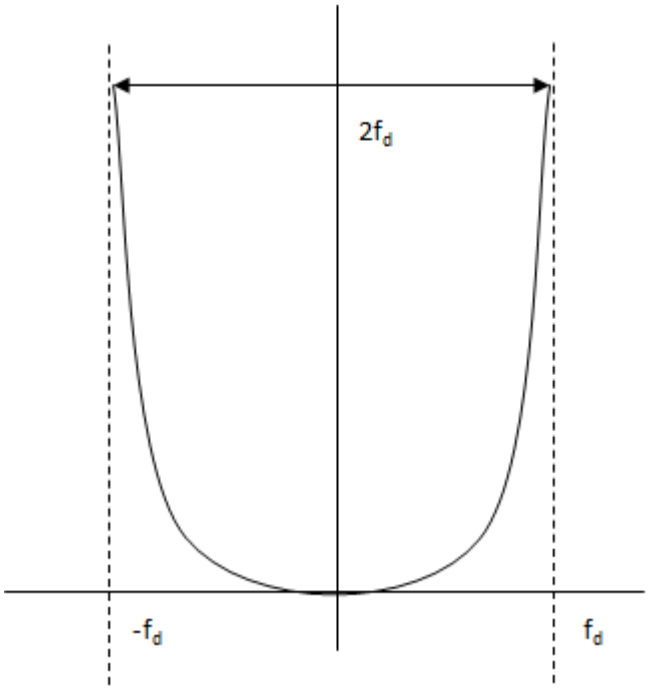

Figure 2.8: Jakes Spectrum [8].

CHAPTER 3: MULTICARRIER MODULATION AND OFDM

3.1 Multicarrier Modulation

Single carrier consists of one carrier for modulating data stream and occupies the entire bandwidth. If a bandwidth 'B' is available for communication, the symbol time will be $T = 1/B$. One symbol is transmitted every T seconds. It is typically two symbols as there is a 'sine' and a 'cosine' term associated with a signal. Symbol rate is the inverse of transmission time which is equal to B. If the available bandwidth is divided into 'N' subcarriers and each data symbol is modulated with the individual subcarrier, the system becomes a multicarrier system. The bandwidth of each subcarrier is $f_n = B/N$ and consequently the spacing between each subcarrier [9]. A typical multicarrier spectrum is shown in Figure 3.1.

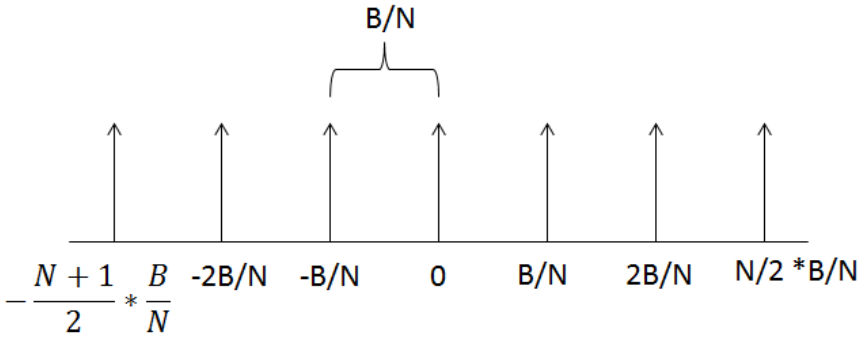

Figure 3.1: Subcarrier Spacing.

3.1.1 Transmission

In multicarrier transmission, the center frequency of the i^{th} subcarrier is given by equation 3.1.

$$f_i = \frac{iB}{N} \tag{3.1}$$

X_i is the data to be transmitted on the i^{th} subcarrier. The modulated data stream is given by equation 3.2.

$$S_i(t) = X_i e^{j2\pi f_i t} \tag{3.2}$$

In a multicarrier system, there are a total of N subcarriers. Hence, N data symbols can be modulated using the N subcarriers. Before transmitting, the N modulated streams are added. The composite transmit signal is given by equation 3.3 [9].

$$S(t) = \sum_i X_i e^{\frac{j2\pi iB}{N}t} \tag{3.3}$$

Figure 3.2 clearly shows the block diagram to implement a multicarrier system.

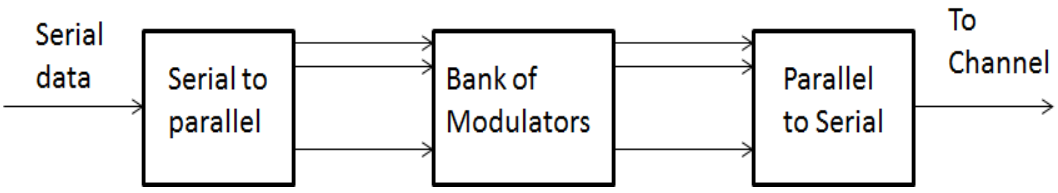

Figure 3.2: Block Diagram of Multicarrier Transmitter System [9].

3.1.2 Reception

The received signal is the transmitted signal accompanied by noise. Ignoring the effect of noise, the received signal is the same as the composite transmitted signal given by equation 3.3.

To get back the original data symbols, each stream is coherently demodulated with its corresponding subcarrier [9]. The process of correlation is done with the l^{th} subcarrier.

$$= \frac{B}{N}\int_0^{\frac{N}{B}} \sum_i X_i e^{\frac{j2\pi iB}{N}t} e^{-\frac{j2\pi lB}{N}t} dt$$

$$= \frac{B}{N}\sum_i \int_0^{\frac{N}{B}} \frac{X_i e^{\frac{j\pi(i-l)B}{N}t} B}{N} t\, dt$$

$$\int_0^{\frac{N}{B}} e^{\frac{j2\pi(i-l)B}{N}t} = \begin{cases} 0 & if\ i \neq l \\ \frac{N}{B} & if\ i = l \end{cases}$$

All subcarriers except l^{th} subcarrier are orthogonal to the l^{th} subcarrier. Hence we can correlate with $e^{-j2\pi f_l t}$. After demodulation with l^{th} coherent subcarrier, we get back the original data stream [9]. The block diagram of an MCM receiver is shown in Figure 3.3.

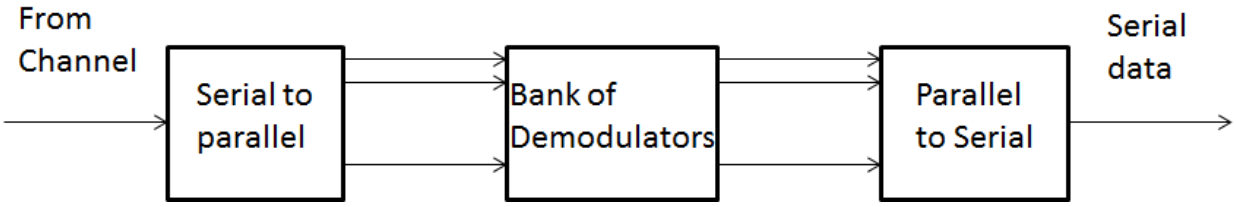

Figure 3.3: Block Diagram of Multicarrier Receiver System [9].

The window of time associated with detection of this multicarrier signal is N/B, which is the time period of integration [9]. Hence, multicarrier modulation transmits N symbols using N subcarriers in time period N/B. The symbol rate is N/(N/B) = B. The net symbol rate using single-carrier vs. multicarrier modulation has not changed. Therefore, nothing has been achieved in terms of symbol rate [9].

3.2 OFDM

Implementing N bank of modulators/correlators and demodulators/decorrelators is a very difficult task as it leads to phase offsets and also increases the cost required to install 2N oscillators [9]. However, there was a key advancement made by Weinstein and Ebert in 1971 at Bell Labs [10]. The Nyquist sampling rate of a multicarrier system is B. The multicarrier system is band limited to B. Consider the u^{th} sample in the system which is given by equation 3.4.

$$S(uT_s) = x(u) = \sum_i X_i e^{\frac{j2\pi iB}{N}\frac{U}{B}} = \sum_i X_i e^{\frac{j2\pi iU}{N}} \tag{3.4}$$

From equation 3.4, it is evident that the output samples are the IDFT of the information symbols. This theory formulated by Weinstein and Ebert provided a breakthrough in modeling the OFDM system. The IDFT and DFT operations replace the modulators and demodulators, making it very efficient. In practice, the IDFT and DFT are implemented by IFFT and FFT operations in the digital signal processor. This proposed scheme of generating the multicarrier transmit signal has a much lower implementation complexity compared to the bank of correlators [9]. Such a system is termed as OFDM. The name orthogonality is used as OFDM uses orthogonal subcarriers instead of random subcarrier frequencies, making it much easier to demodulate on the receiver due to the orthogonality principle.

The coherence bandwidth in outdoor channels for a 3G/4G system is about 300 kHz. The bandwidth for an OFDM system is about 2 GHz. It can be clearly seen that bandwidth is very much higher than the coherence bandwidth. This leads to inter-symbol interference (ISI). OFDM employs smart methods to combat the issue of ISI or IBI.

3.2.1 Transmitter

The block schematic of an OFDM transmitter is demonstrated in Figure 3.4. The raw data bits are modulated using various digital modulation schemes like QAM, PSK and BPSK. Since OFDM focusses on parallel transmission of data, the serial data after modulation is converted into parallel data. The size of the parallel data depends upon the number of subcarriers used. The parallel symbol stream is then sent to the modulator block, which is now replaced by the IFFT operation. Here, each data symbol is modulated with its corresponding subcarrier. The parallel modulated data is now converted into serial data and it goes into the cyclic prefix module. In this block, the last few symbols are copied and attached at the beginning of the OFDM symbol. This is done mainly to avoid the effects of multipath propagation and fading. After the addition of cyclic prefix, the data is sent out into the channel which is to be captured by the receiver.

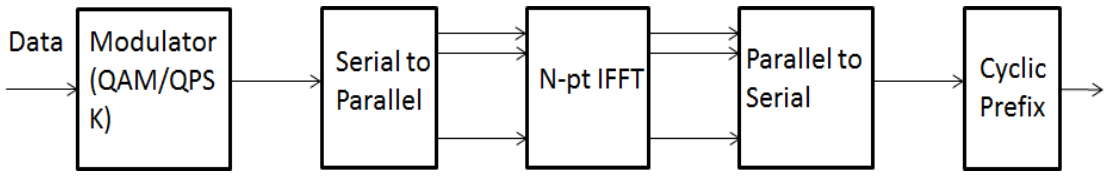

Figure 3.4: OFDM Transmitter Block Diagram [9].

N represents the number of subcarriers. Typically the number of subcarriers is a power of 2. In practical applications, the number of subcarriers is equal to $2^x * 3^y * 5^z$, where x, y and z's are integers.

3.2.2 Receiver

At the receiver, the opposite procedure is done compared to the transmitter. The symbols received are first deprived of the cyclic prefix. The serial symbol stream is converted into a

parallel symbol stream by using the multiplexer or serial to parallel converter. The parallel symbol stream is demodulated by using the N-pt FFT operation. FFT is a correlator or a frequency domain sampler. The parallel symbol stream after the FFT operation is demodulated to the baseband and serialized, which goes to various applications. Figure 3.5 shows the schematic block diagram of a typical OFDM receiver.

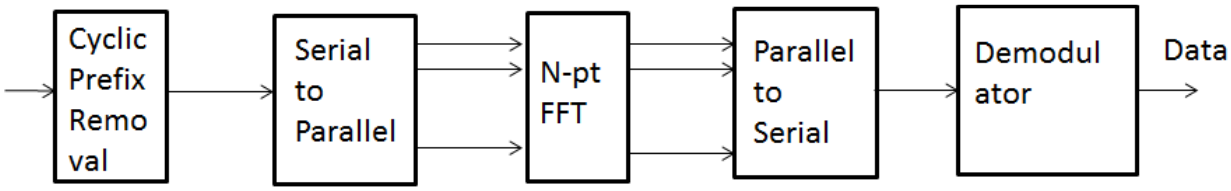

Figure 3.5: OFDM Receiver Block Diagram [9].

CHAPTER 4: PAPR AND INTRODUCTION TO SCFDMA

4.1 Peak to Average Power Ratio (PAPR)

4.1.1 Cause of PAPR

The major drawback of using OFDM in the uplink is the presence of PAPR. The summation operation of the closely spaced subcarriers cause high peak signals compared to the average peaks. The IFFT operation in the transmitter causes PAPR. The complex OFDM symbol is given by equation 4.1.

$$x(k) = \frac{1}{N}\sum_{i=0}^{N-1} X(i) e^{\frac{j2\pi ki}{N}} \tag{4.1}$$

X(i) are the modulated symbols to be given to the IFFT block and x(k) are the k^{th} IFFT sample. The average power of the signal mentioned in equation 4.1 is given by equation 4.2.

$$Average\ Power = E\{|x(k)|^2\} = \frac{1}{N^2}\sum_{i=0}^{N-1} E\{|X(i)|^2\} E\{\left|e^{\frac{j2\pi ki}{N}}\right|^2\}$$

$$= \frac{1}{N^2}\sum_{i=0}^{N-1} E\{|X(i)|^2\} = \frac{1}{N^2}\sum_{i=0}^{N-1} a^2$$

$$= \frac{1}{N^2} a^2 N = \frac{a^2}{N} \tag{4.2}$$

The average power of transmission is a^2/N. The peak transmission power is given by equation a^2. PAPR, which is a fraction of peak power in average power, is given by equation 4.3.

$$PAPR = \frac{Peak\ Power}{Average\ Power} = \frac{a^2}{\frac{a^2}{N}} = N \tag{4.3}$$

From equation 4.3 it is seen that PAPR depends upon the number of subcarriers. PAPR increases proportionally as the number of subcarriers in IFFT increases. It mainly occurs due to the IFFT preprocessing. Data symbols across subcarriers can add up constructively to produce a signal with a very high peak value. In an OFDM system with 256 subcarriers and modulation of 16 QAM, the PAPR is about 10dB, i.e., 10 times peak power compared to average power. PAPR increases as the number of subcarriers in the IFFT preprocessing increases. PAPR is characterized by the complementary cumulative distribution function (CCDF). It gives a measure about the probability that PAPR value is below a given threshold. CCDF function is described by equation 4.4.

$$F_X'(x) = P(X \geq x) \tag{4.4}$$

$$CCDF = 1 - CDF$$

Figure 4.1 shows the PAPR curves for an OFDM system with 256, 128 and 64 subcarriers with a modulation of 16 QAM. From a typical CCDF curve, which follows a chi-square distribution, PAPR can be read as the probability that a certain PAPR value will exceed a threshold for N subcarriers. From Figure 4.1, the probability that PAPR will exceed 10dB for N = 256 is 0.01 or 1% CCDF. From Figure 4.1 it can be seen that as the number of subcarriers increases from 64 to 256, PAPR is also increasing proportionally. This gradual increase can cause adverse effects which are dealt in the later sections of this chapter.

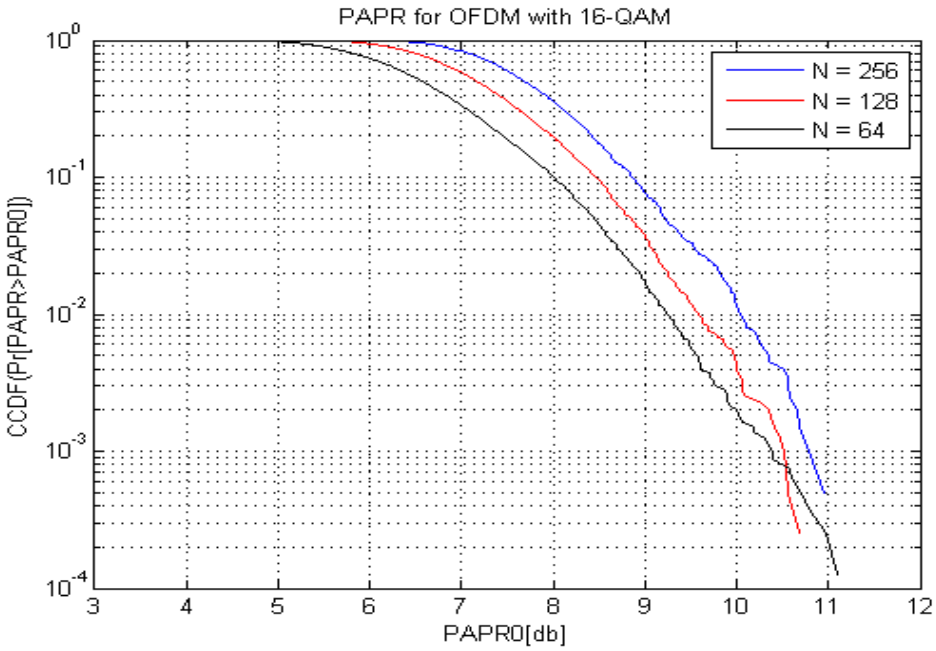

Figure 4.1: PAPR Curves for Different N Values.

However, the type of modulation scheme employed has no effect on PAPR, which can be seen in Figure 4.2.

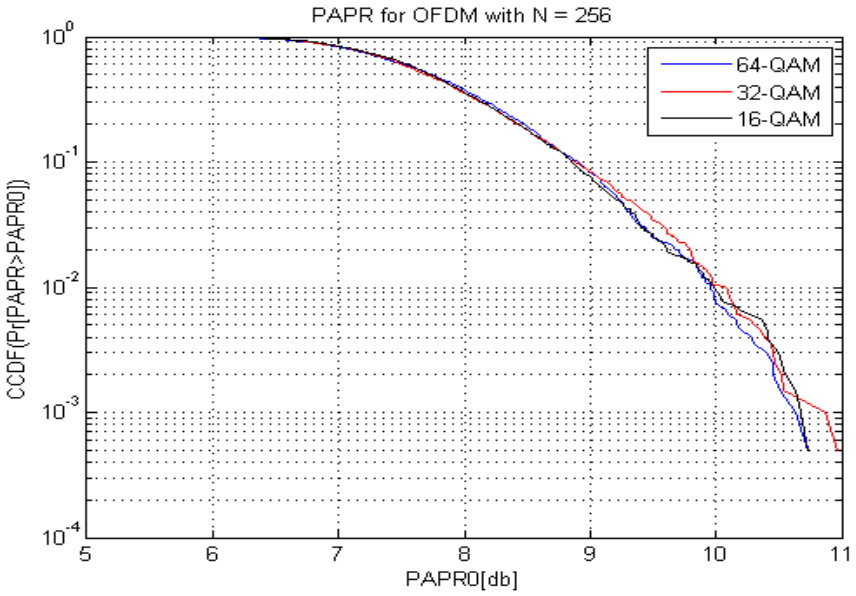

Figure 4.2: PAPR Curves for Various Modulation Schemes.

4.1.2 Effect of PAPR

Power amplifiers with certain dynamic range are used in the transmitter before transmitting the signal. Presence of high peaks in the signal will make the peak level go beyond the average level point. The average level point can also be called as the Q-point. When the peak level goes beyond the average level, the amplifier goes into the saturation region. It is no longer functioning in the linear range. The Q-point is now in the saturation range. In this region, the amplifier is totally saturated leading to signal clipping. The clipped signal has some information loss and the shape of the clipped signal is different from the original one. Amplifier saturation leads to nonlinearity, distortion and inter-carrier interference (ICI). Orthogonality among subcarriers is lost due to clipping, which leads to a very low signal to noise ratio (SNR). Figure 4.3 shows the typical characteristics of an amplifier.

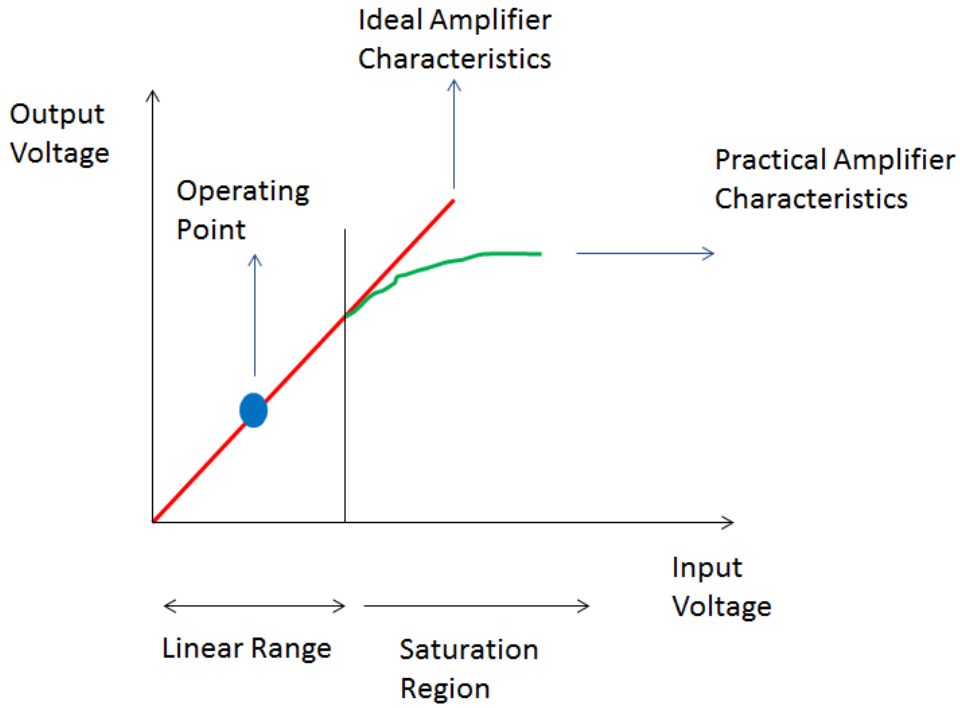

Figure 4.3: Amplifier Characteristics.

4.2 Introduction to SCFDMA

Various algorithms have been developed to tackle PAPR problem in OFDM system. Coding, clipping and scrambling techniques were proposed to reduce PAPR. However, these techniques require complex transmitter and receiver structures. This would increase the cost of hardware required and hence make it costly for the user to acquire it. The overall performance or throughput using these techniques is very less, leading to very low SNR and capacity issues. The computational complexity also becomes high, leading to lower data rates and lower transmission speeds. PAPR in the uplink transmission is a very serious issue as it leads to increased cost of power amplifiers. This directly causes an increase in the handset cost thus making OFDM a very inefficient technology for uplink transmission. In order to overcome these problems, 3GPP introduced single-carrier frequency division multiple access (SCFDMA) for uplink communication in long-term evolution (LTE) [4]. As the name itself says, it is a single-carrier technique which derives many or most of OFDM properties to successfully overcome the effects of PAPR.

4.2.1 Concept of PAPR Reduction

As mentioned in Section 4.1.1, N-pt IFFT operation leads to PAPR. By countering the N-pt IFFT operation, PAPR can be reduced effectively. One way of doing this is to place an N-pt FFT block before the N-pt IFFT block. The two blocks cancel out each other and we get a PAPR value of 1, which is equal to that of a single-carrier system [9]. Moreover, a system with an N-pt FFT followed by an N-pt IFFT is effectively a single-carrier system. In earlier chapters it was

shown that single-carrier systems suffer from ISI. The modified OFDM transmitter block is shown in Figure 4.4.

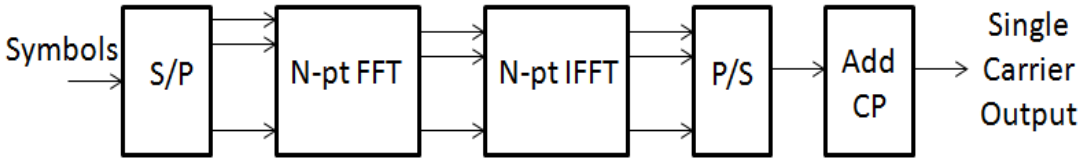

Figure 4.4: Modified OFDM Transmitter [9].

Completely moving to a single-carrier system is not recommended as ISI is predominant. OFDM properties must be retained in order to mitigate ISI. Hence, instead of using an N-pt FFT an M-pt FFT is used, where M < N.

4.2.2 SCFDMA Transmission in Uplink

The basic difference between the transmission in OFDM and SCFDMA is that in OFDM data is modulated onto subcarriers and sent over multiple carriers, whereas in SCFDMA, data of each user is mapped onto their allotted subcarriers and sent over a single carrier. In fact, all users transmit on the same carrier. This reduces the burden on the base station as it can tune only to one carrier frequency. The base station can put more power into managing multiuser transmission in the downlink communication. A typical SCFDMA transmission in the uplink is shown in Figure 4.5.

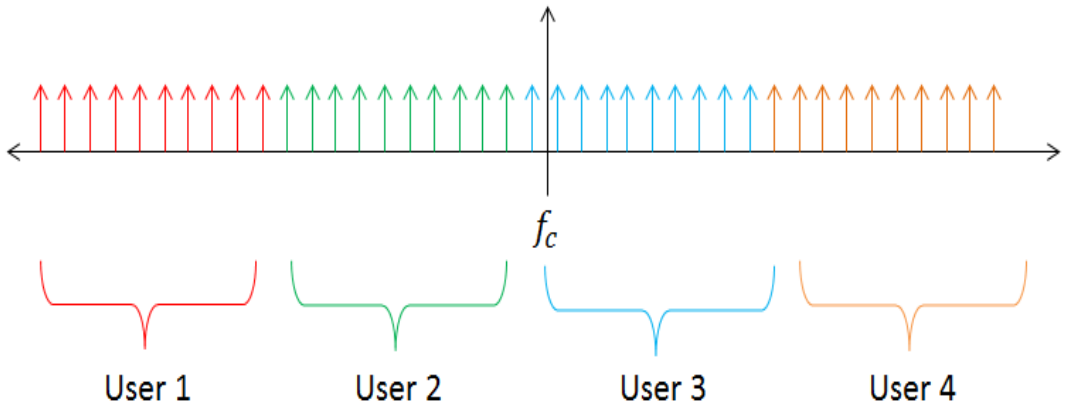

Figure 4.5: Multiuser SCFDMA Transmission in Uplink.

There are a total of four users who are in the network. Forty subcarriers are allotted where each user is given 10 subcarriers. From the figure it can be seen that each user occupies a different portion of bandwidth and different subcarriers but transmit data with the same carrier frequency. This is the basis of communication in single-carrier systems.

4.2.3 Transmitter of SCFDMA

The transmitter block diagram for an SCFDMA system in the uplink is demonstrated in Figure 4.6.

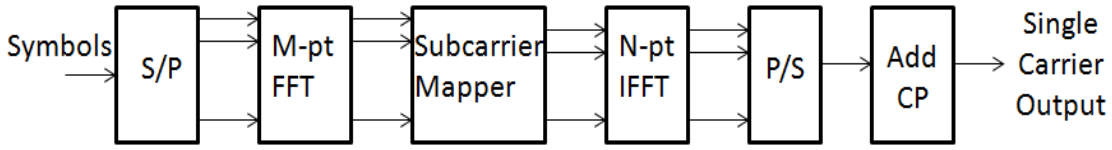

Figure 4.6: SCFDMA Transmitter [9].

The block diagram is similar to that of an OFDM system except for the new M-pt FFT and subcarrier mapper block. The different mapping techniques are explained in the later

sections and the new mapping scheme is also proposed. The parallel outputs are given to the IFFT block to get the time domain signal output. Cyclic prefix is added to combat multipath propagation and ISI. A single-carrier signal is generated and sent over the channel.

4.2.4 Receiver of SCFDMA

The receiver block diagram for SCFDMA is given in Figure 4.7. The structure is similar to that of an OFDM receiver. However, there are two more blocks added in order to compensate for the transmitter blocks. They are the de-mapper and M-pt IFFT block corresponding to the transmitter.

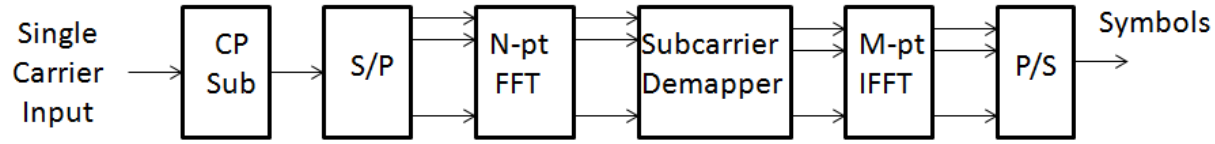

Figure 4.7: SCFDMA Receiver [9].

Upon signal reception, cyclic prefix is removed which contains ISI symbols. As the signal progresses, it is given to the N-pt FFT block. It is then de-mapped according to the corresponding scheme employed at the transmitter. The signal then goes to the M-pt IFFT block. The symbols are then demodulated and the corresponding data bits are then fed to various applications.

CHAPTER 5: SUBCARRIER MAPPING AND PROPOSED TECHNIQUE

5.1 Localized FDMA (LFDMA)

The symbols which have to be mapped onto the subcarriers are first fed to the M-pt DFT block. The FFT output symbols are passed to a mapper block. In localized setting, the symbols are mapped onto the adjacent subcarriers which occupy the SCFDMA frame. They can be mapped anywhere in the frame, i.e., for the starting subcarriers, ending subcarriers or the subcarriers in the middle of the frame. The remaining subcarriers are marked with zeros. These subcarriers can be occupied by another user terminal located in the vicinity of the base station. A typical LFDMA frame for six user symbols that have to be loaded onto 12 subcarriers is shown in Figure 5.1 [4].

Figure 5.1: LFDMA Frame Structure.

The expected PAPR for such a frame structure will be less than the conventional OFDM system as only half the subcarriers are occupied, leaving the remaining subcarriers with zeros. For four users with 10 subcarriers each, the LFDMA transmission frame is shown in Figure 5.2. From the figure, it is clear that in this mapping scheme each user occupies contiguous bandwidth locations.

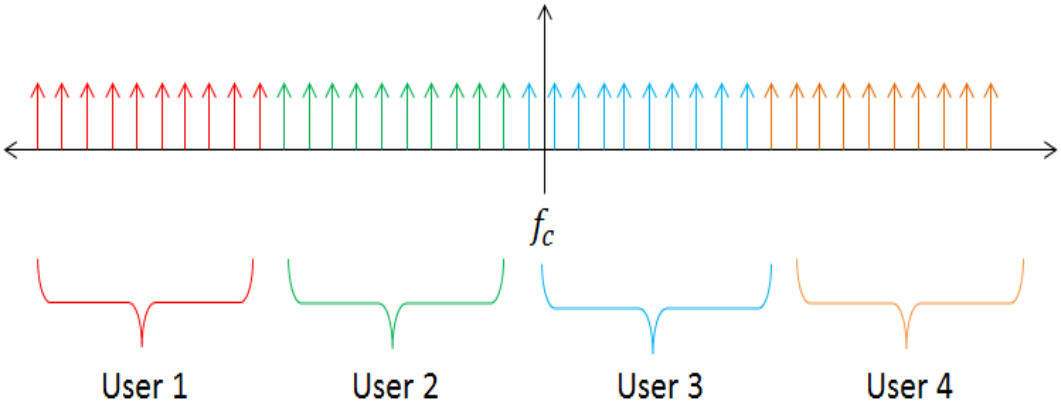

Figure 5.2: Multiuser LFDMA Transmission.

The PAPR comparison for LFDMA and OFDM with N = 128 and 16-QAM is shown in Figure 5.3. From the Figure it can be concluded that the PAPR for a CCDF of 1% in an OFDM and SCFDMA system with LFDMA mapping is approximately 9.7dB and 7.8dB. Hence, there is a decrease of 2dB in PAPR using the LFDMA mapping. From Figure 5.1, it can be seen that LFDMA mapping is easy to implement for the base station as the symbols occupy contiguous bandwidth locations. Multiuser diversity, which is also known as base station scheduling, can be achieved. However, LFDMA systems suffer from frequency diversity as the symbols are not spread over the entire frequency band [3].

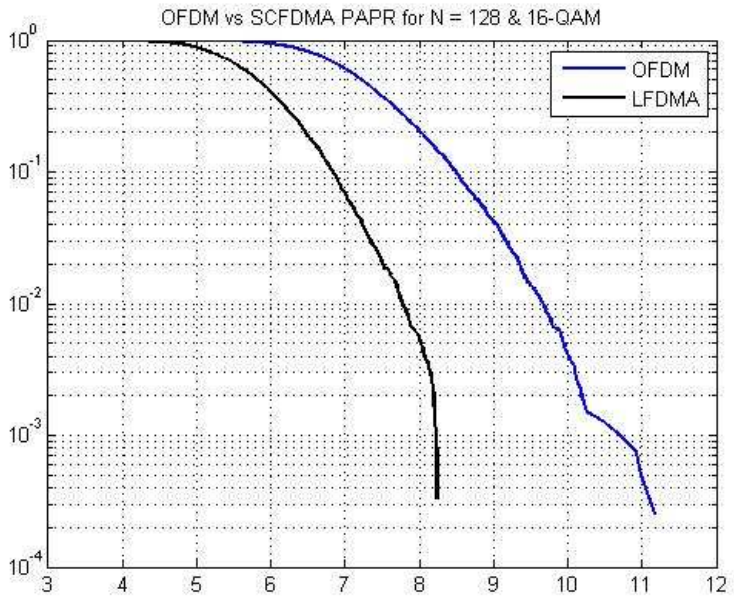

Figure 5.3: PAPR of OFDM vs. LFDMA.

5.2 Interleaved FDMA (IFDMA)

The symbols which have to be mapped onto the subcarriers are first fed to the M-pt DFT block. The FFT outputs are then given to the mapper block. In interleaved setting, the symbols are mapped onto alternating subcarriers which occupy the SCFDMA frame. The position of symbols at the alternating places depends upon the number of users in the communication link and the number of symbols. The remaining subcarriers are marked with zeros. These subcarriers can be occupied by another user terminal located in the vicinity of the base station. An IDMA frame for a user with six symbols that have to be loaded onto 12 subcarriers is shown in Figure 5.4 [4].

Figure 5.4: IFDMA Frame Structure.

For four users with 10 subcarriers each, the IFDMA transmission frame is shown in Figure 5.5. From the figure, it is clear that in this mapping scheme, each user occupies alternating positions, depending upon the number of users in the system.

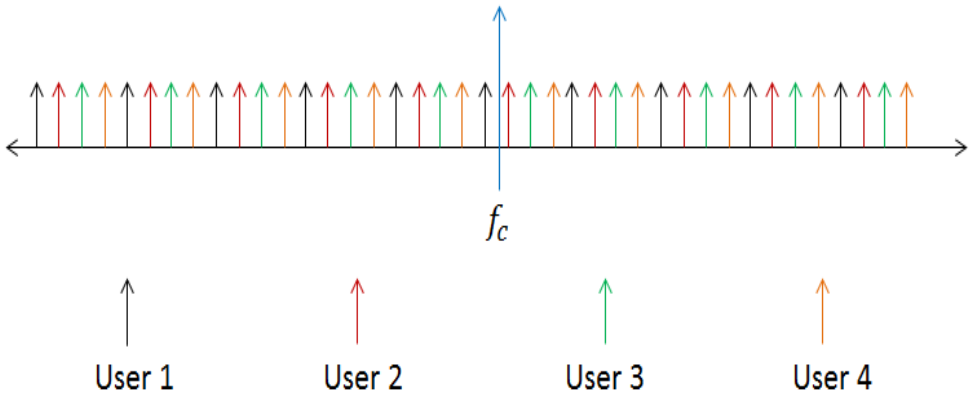

Figure 5.5: Multiuser IFDMA Transmission.

The expected PAPR for such a frame structure will be much less than the OFDM system and considerably less than the LFDMA system as the symbols are placed far apart. Hence, there is less chance for the peaks to get added up. The PAPR comparison for IFDMA and OFDM with N = 128 and 16-QAM is shown in Figure 5.6.

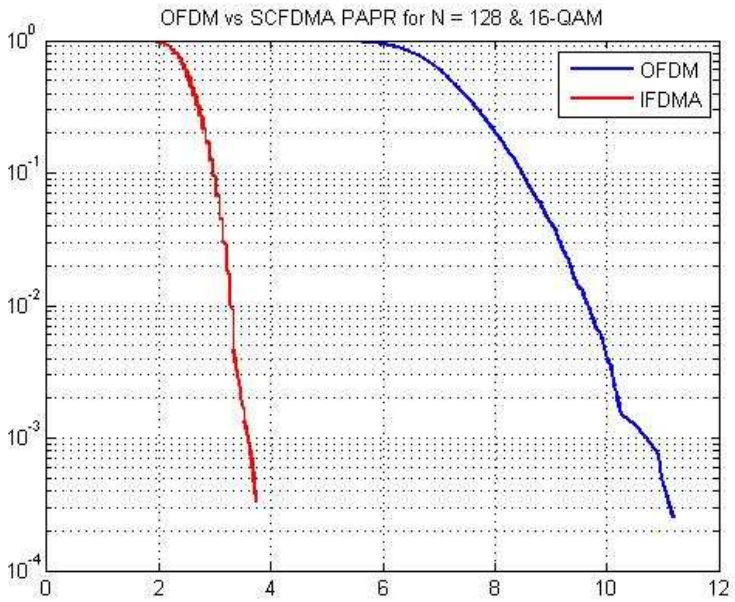

Figure 5.6: PAPR of OFDM vs. IFDMA.

From the Figure it can be concluded that the PAPR for a CCDF of 1% in an OFDM and SCFDMA system with IFDMA mapping is approximately 9.8dB and 3.2dB. Hence, there is a decrease of 6.4dB in PAPR using the IFDMA mapping. From Figure 5.4, it can be seen that IFDMA mapping is difficult to implement for the base station as the symbols are spread in the entire bandwidth. User scheduling becomes very tough. However, IFDMA systems provide the advantage of frequency diversity [3].

5.3 Existing Hybrid FDMA (HFDMA)

As mentioned earlier, HFDMA was developed by F.S. Al-kamali [4]. It uses both the LFDMA and IFDMA modes. Symbols of one user are mapped onto the subcarriers as shown in the mapping. The remaining subcarriers are marked with zeros. These subcarriers can be

occupied by another user terminal located in the vicinity of the base station. A typical HFDMA frame for six user symbols that have to be loaded onto 12 subcarriers is shown in Figure 5.7.

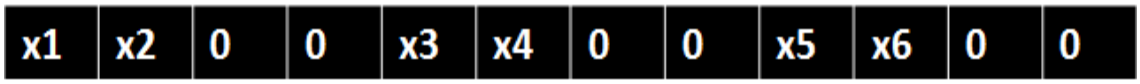

Figure 5.7: HFDMA Frame Structure [3].

The expected PAPR for such a frame structure will be much less than the OFDM system and in between localized and interleaved modes. The PAPR comparison for HFDMA with N = 128 and 16-QAM is shown in Figure 5.8.

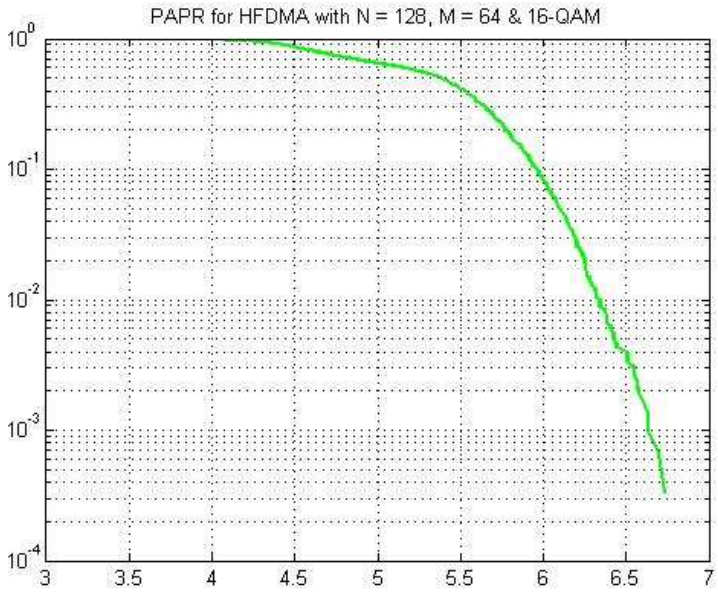

.

Figure 5.8: PAPR with HFDMA Mapping.

From the figure it can be seen that for a CCDF of 1%, the PAPR is about 6.3dB. This value is in between values achieved with the localized and interleaved modes.

5.4 Proposed Mapping Technique

A modified hybrid mapping technique is designed which used both the interleaved and localized designs. For the first half of the user's bandwidth, localized mode is employed while the second half is filled with the interleaved mode. The entire frame is repeated for the whole bandwidth. Using this technique, both frequency diversity and multiuser diversity can be achieved while reducing the PAPR at the same moment. The MHFDMA frame structure is demonstrated in Figure 5.9.

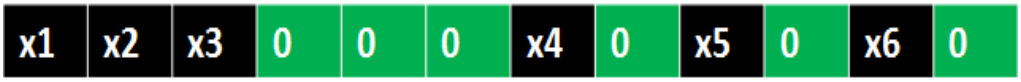

Figure 5.9: MHFDMA Frame Structure.

The expected PAPR for the new structure is expected to be in between the PAPR value obtained for LFDMA and IFDMA. The PAPR comparison for MHFDMA and OFDM with N = 128 and 16-QAM is shown in Figure 5.10. The PAPR in OFDM is about 9.8dB while in MHFDMA it is about 6dB for a CCDF of 1%. The reduction is about 3.6-3.8dB. The PAPR for MHFDMA is 0.2-0.3dB less than the existing HFDMA technique. This may be a statistical error. More than half the battery power is saved using the MHFDMA structure. The plot of MHFDMA vs. OFDM is shown in Figure 5.10 while the comparison of all the techniques is shown in 5.11. It can be inferred that MHFDMA provides better PAPR reduction than OFDM and LFDMA but less than IFDMA. However, the implementation overhead is less than IFDMA but greater than LFDMA.

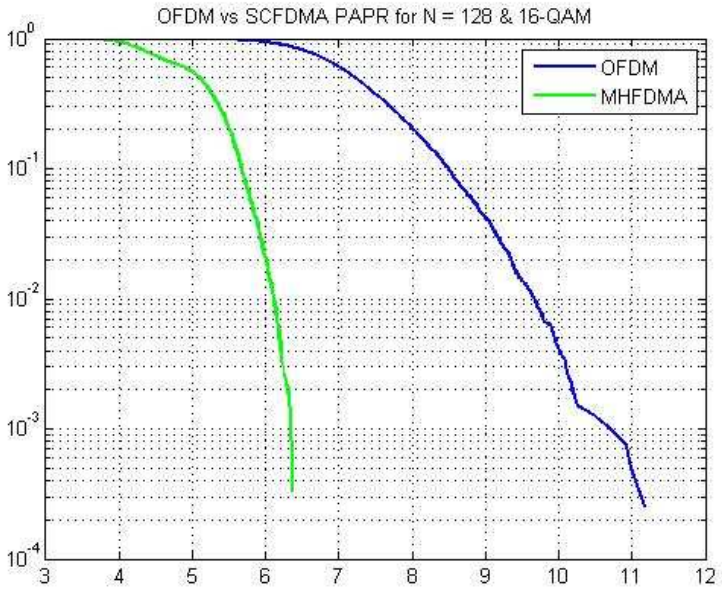

Figure 5.10: MHFDMA vs. OFDM.

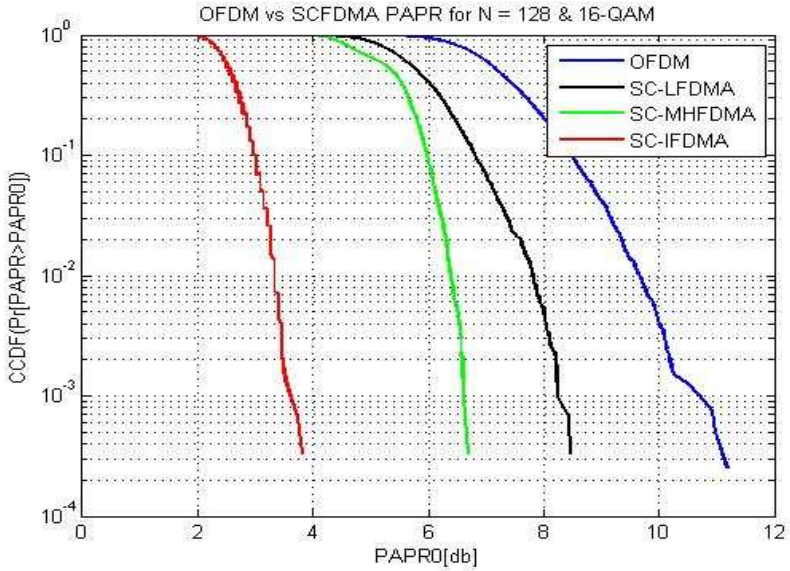

Figure 5.11: A Comparative Study.

The BER performance using the three techniques in the absence of Doppler is shown in Figure 5.12. Only User 1 is kept ON while User 2 is kept OFF. It can be observed that all three

schemes have a similar BER performance as shown in Figure 5.12; 8000 SCFDMA symbols are used in the simulation.

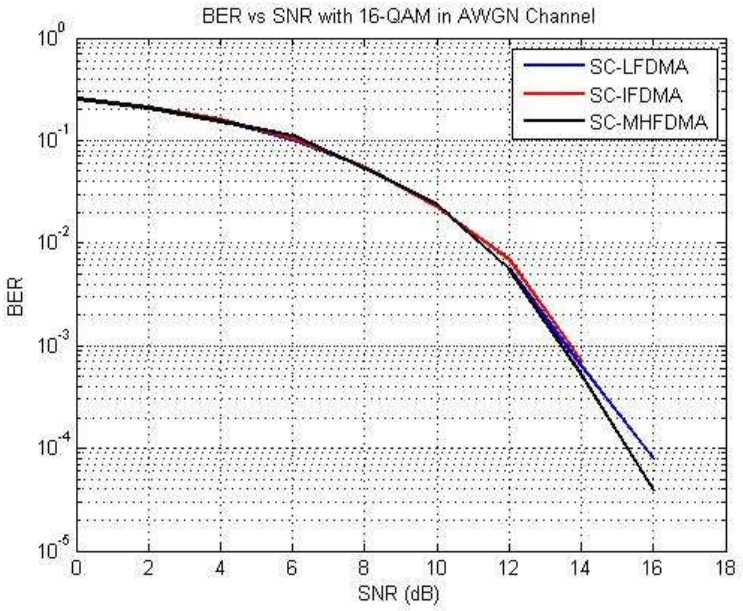

Figure 5.12: BER for SCFDMA with 16-QAM.

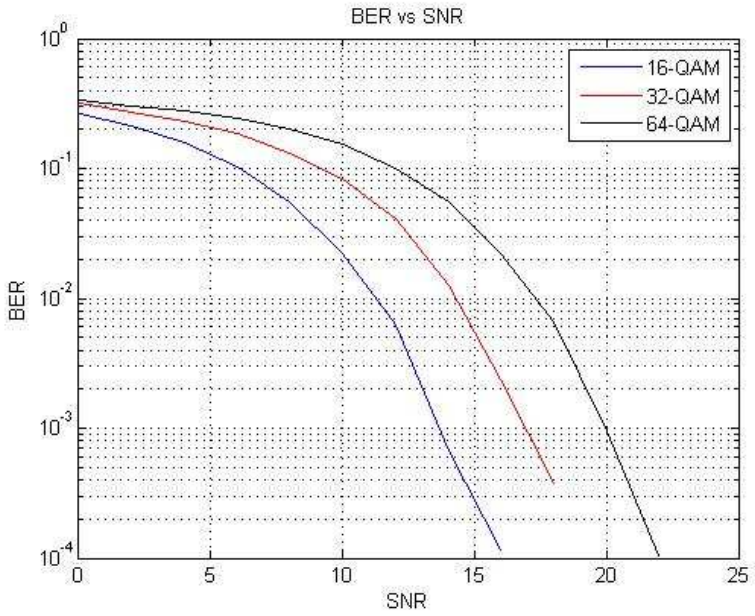

Figure 5.13: BER for Various Modulation Schemes for User 1 in AWGN Channel.

CHAPTER 6: SIMULATION RESULTS AND ANALYSIS

The BER for the three mapping techniques are simulated for four users with 1%, 0.1% and 0.01% Doppler values. Sixteen QAM modulation scheme is adopted with 1024 subcarriers, where each user is allotted 256 subcarriers. Multipath propagation is considered with four channel taps at different time instants and average path power loss. The BER values are tabulated considering a value of 0.001, i.e., 1 error bit in every 1000 bits. The BER for each user is identical to the other three users. Figure 6.1 depicts the BER for four users in an AWGN channel without Doppler. However, percentage Doppler values must be considered based upon the symbol rate received at the receiver end. The bandwidth in LTE systems is 5MHz which gives a maximum feasible symbol rate of 10Msym/sec. For a Doppler frequency of 150 Hz, the corresponding percentage Doppler is 0.0015%. Simulations are shown for this particular percentage Doppler value as it is the practical situation. All simulations henceforth are carried out with 10000 SCFDMA symbols.

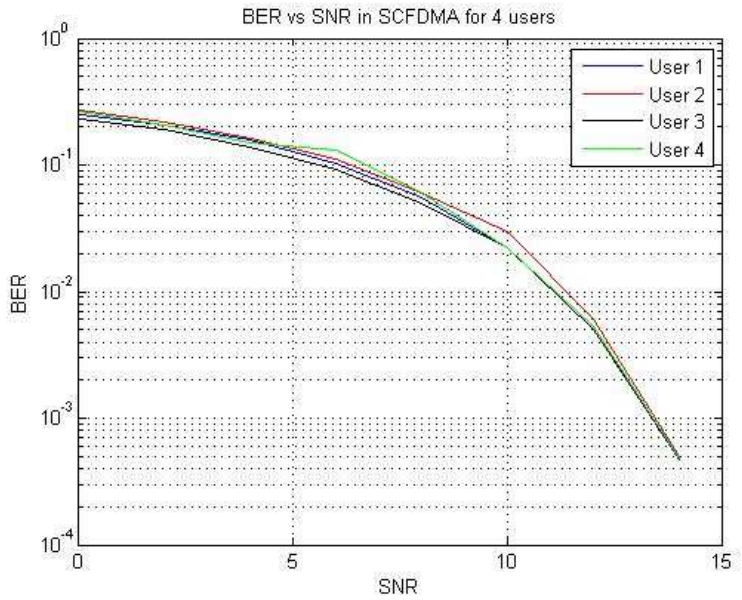

Figure 6.1: BER vs SNR for 4 Users in AWGN Channel.

6.1 IFDMA Simulations

The IFDMA frame structure is simulated for the parameters mentioned earlier. Figure 6.2 shows the BER performance in case of zero Doppler, 1% Doppler, 0.1% Doppler and 0.01% Doppler. The respective SNR values to obtain a BER of 0.001 are 13.3dB, 17.2dB, 15.2dB and 14.2dB for no Doppler, 1%, 0.1% and 0.01% Doppler. Figure 6.3 shows the BER performance for 0.0015% Doppler when all four users are ON. It can be seen BER performance for all users is similar, i.e., about 14dB.

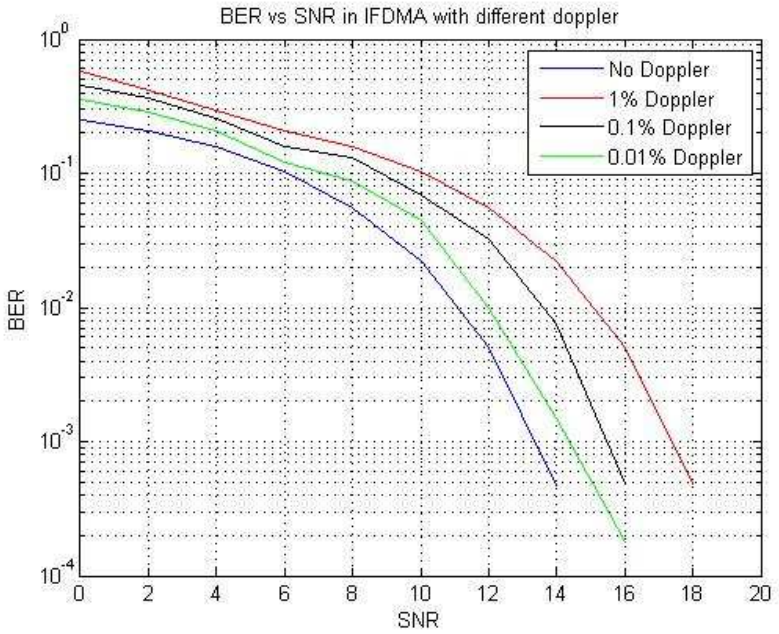

Figure 6.2: BER vs SNR in IFDMA for User 1 in 4-Tap Rayleigh Channel.

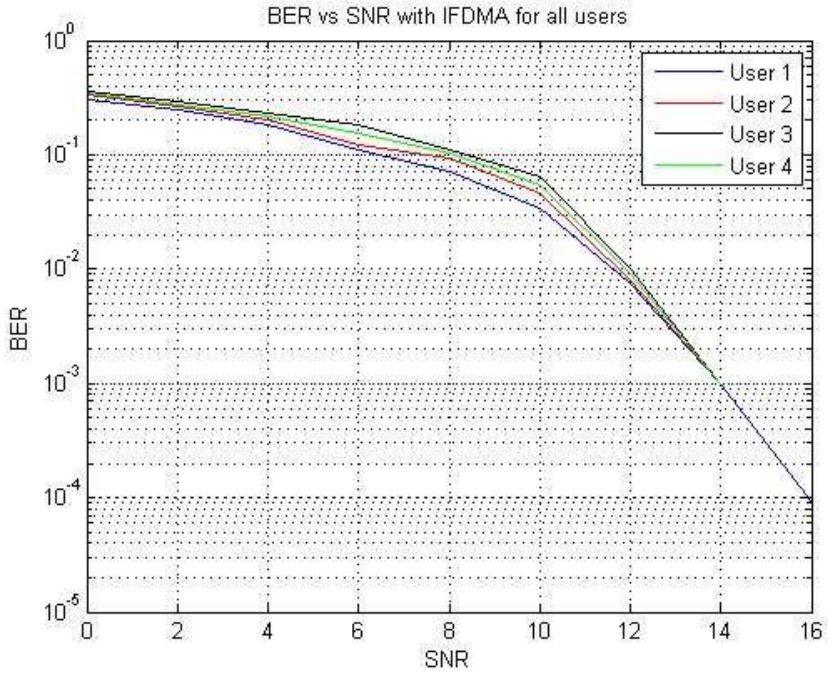

Figure 6.3: BER vs SNR in IFDMA for 0.0015% Doppler in 4-Tap Rayleigh Channel.

6.2 LFDMA Simulations

The LFDMA frame structure is simulated for the parameters mentioned earlier. Figure 6.4 shows the BER performance in case of zero Doppler, 1% Doppler, 0.1% Doppler and 0.01% Doppler. The respective SNR values to obtain a BER of 0.001 are 13.2dB, 16.8dB, 14.9dB and 13.9dB for no Doppler, 1%, 0.1% and 0.01% Doppler. Figure 6.5 shows the BER performance for 0.0015% Doppler when all four users are ON. It can be seen BER performance for all users is similar, i.e., about 14dB.

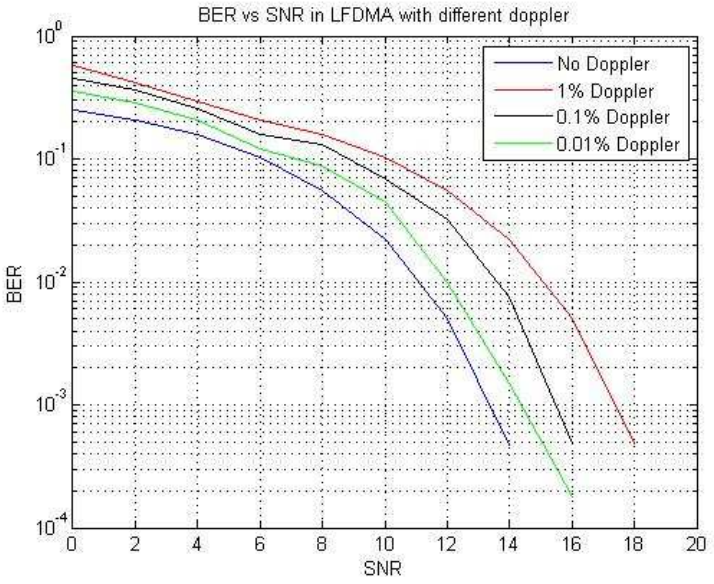

Figure 6.4: BER vs SNR in LFDMA for User 1 in 4-Tap Rayleigh Channel.

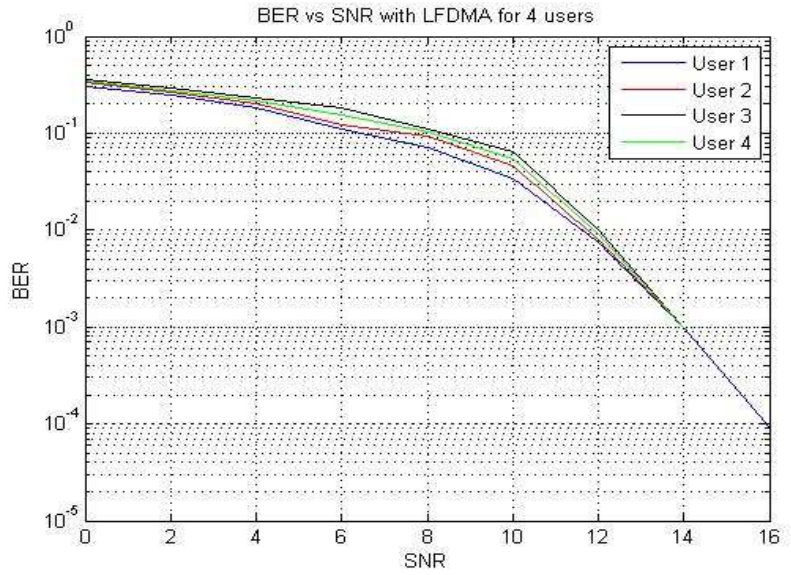

Figure 6.5: BER vs SNR in LFDMA for 0.0015% Doppler in 4-Tap Rayleigh Channel.

6.3 MHFDMA Simulations

The MHFDMA frame structure is simulated for the parameters mentioned earlier. Figure 6.6 shows the BER performance in case of zero Doppler, 1% Doppler, 0.1% Doppler and 0.01% Doppler. The respective SNR values to obtain a BER of 0.001 are 13.2dB, 17.1dB, 15.1dB and 14.0dB for no Doppler, 1%, 0.1% and 0.01% Doppler. Figure 6.7 shows the BER performance for 0.0015% Doppler when all four users are ON. It can be seen BER performance for all users is similar, i.e., about 14dB.

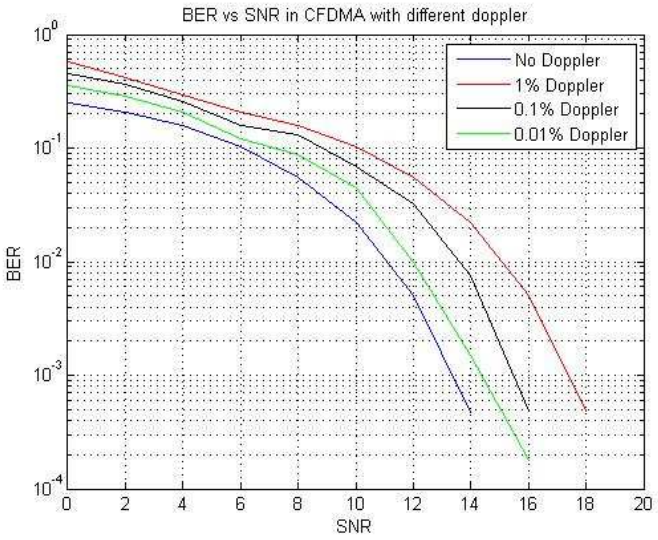

Figure 6.6: BER vs SNR in MHFDMA for User 1 in 4-Tap Rayleigh Channel.

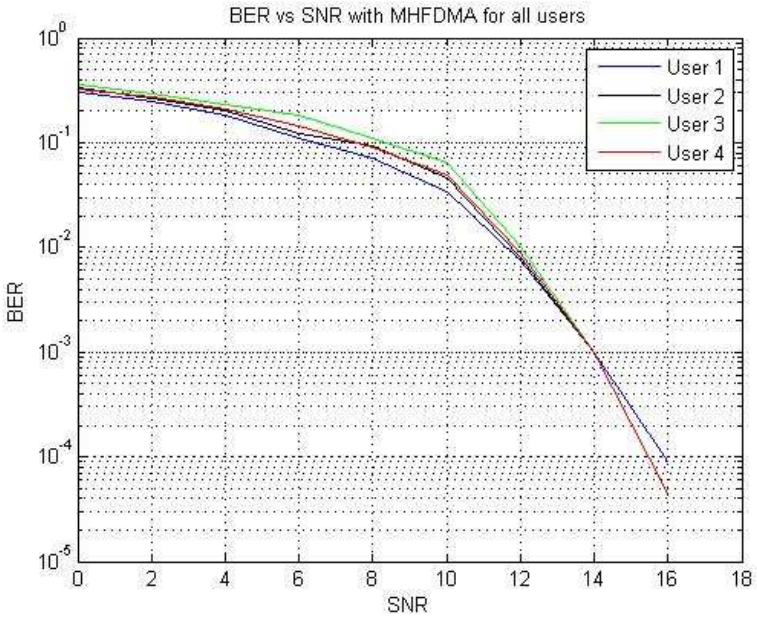

Figure 6.7: BER vs SNR in MHFDMA for 0.0015% Doppler in 4-Tap Rayleigh Channel.

6.4 Comparative Analysis

Table 6.1 shows the comparative results of all the three mapping techniques. The number of subcarriers used is 512 with 16-QAM modulation scheme. All SNR values are tabulated in dB for a BER of 0.001. A single user is considered as the SNR for all the users is found to be the same.

Table 6.1: Comparative Analysis of All Techniques

	0 Doppler	1% Doppler	0.1% Doppler	0.01% Doppler	0.0015% Doppler
LFDMA	13.3 dB	17.2 dB	15.2 dB	14.2 dB	14 dB
IFDMA	13.3 dB	16.8 dB	14.9 dB	13.9 dB	14 dB
MHFDMA	13.3 dB	17.1 dB	15.1 dB	14.0 dB	14 dB

From the table it is concluded that as the transmission rate increases, the SNR comes closer to the no Doppler case. The SNR for IFDMA mapping case is slightly lower than the other two techniques. However, the PAPR in LFDMA is high compared to the other two mapping techniques. The modified hybrid technique solves the issue by providing an average PAPR value with the same BER value. Moreover, the modified hybrid technique provides both multiuser diversity (provided by LFDMA) and frequency diversity (provided by IFDMA).

CHAPTER 7: CONCLUSION AND FUTURE WORK

7.1 Conclusion

Moving stations produce Doppler which causes a stationary time invariant channel to become a time varying channel. Due to Doppler, the frequency of the wave is changed which causes ICI. The BER is considerably reduced due to the loss of orthogonality among subcarriers. To mitigate this effect, transmission rate is increased which significantly reduces the effect of Doppler.

The SCFDMA system is simulated with different subcarrier mapping techniques like LFDMA, MHFDMA and IFDMA. LFDMA has a high PAPR compared to MHFDMA followed by IFDMA. High PAPR is undesirable as it increases the cost of mobile equipment. Considering the implementation issue, LFDMA is easy to implement followed by MHFDMA and IFDMA. LFDMA only offers only multiuser diversity while IFDMA offers only frequency diversity. The new modified hybrid scheme offers both multiuser and frequency diversity. The modified hybrid scheme also provides a 3dB less PAPR than LFDMA.

The BER performance is evaluated for multiple users employing SCFDMA. It is concluded that the BER is the same using all mapping techniques for various Doppler values. Taking into consideration all the pros and cons, it can be concluded that MHFDMA is a promising technique that can be employed in mobile communication provided the cost issues are considered.

7.2 Future Work

The future work may include employing the single-carrier technique in the downlink transmission of LTE. MIMO-SCFDMA can be established and BER performance can be analyzed and compared with the regular SISO system. Basic PAPR reduction techniques can be added to the modified hybrid scheme to make it even more efficient. Better receiver schematics may be employed to further improve the BER. Space time codes in LTE uplink can be implemented.

REFERENCES

[1] Dwivedi, S.K., Paulus, R., Jaiswal, A.K., and Anil Kumar, April 2014, "Evaluate the PAPR and BER Performance of SCFDMA with NCT Technique," *International Journal of Current Engineering and Technology*, India, E-ISSN 2277-4106, P-ISSN 2347-5161, Vol. 4, No. 2, pp. 1000-1003.

[2] Verma, P., and Sharma, N., September 2012, "IFDMA-Promising Technique for 3G/4G," *International Journal of Electronics and Computer Science Engineering*, P. Verma et al., eds.,India, ISSN 2277-1956, Vol. 1, No. 4, pp. 2207-2216.

[3] Salah, M., Abdel-Fadeel, G., and Nossair, Z.B., May 26-28, 2009, "Peak to Average Power Ratio Reduction in Single Carrier OFDMA Systems," 13th International Conference on Aerospace Sciences & Aviation technology (ASAT-13), ASAT-13-CM-14, Cairo, Egypt.

[4] F.S. Al-kamali, March 2013, "Hybrid Mapping Scheme for Recent Orthogonal FDMA Schemes," *Int. J. Communications, Networks and System Sciences*, Yemen, Vol. 6, No. 3, pp. 149-154, http://dx.doi.org/10.4236/ijcns.2013.63018.

[5] Myung, H.G., January 2007, "Single Carrier Orthogonal Multiple Access Technique for Broadband Wireless Communications," Ph.D. thesis, http://www.scribd.com/doc/76499421/Hyung-G-Myung-PhD-Thesis

[6] Myung, H.G., and Goodman, D.J., 2008, "Single Carrier FDMA: A New Air Interface for Long Term Evolution," John Wiley & Sons, Ltd., New York, 2008. doi: 10.1002/9780470758717

[7] Jagannatham, A.K., "Wireless Channel and Fading." Lecture 2 in Advanced 3G and 4G Wireless Mobile Communications (online course). Indian Institute of Technology, Kanpur, India. Retrieved 01/10/2014. http://nptel.ac.in/courses/117104099

[8] Jagannatham, A.K., "Wireless Channel and Delay Spread." Lecture 9 in Advanced 3G and 4G Wireless Mobile Communications (online course). Indian Institute of Technology, Kanpur, India. Retrieved 01/10/2014. http://nptel.ac.in/courses/117104099

[9] Jagannatham, A.K., “Introduction to OFDM and Multicarrier Modulation.” Lecture 27 in Advanced 3G and 4G Wireless Mobile Communications (online course). Indian Institute of Technology,Kanpur, India. Retrieved 01/10/2014. http://nptel.ac.in/courses/117104099

[10] Weinstein, S., Ebert, P., October 1971, "Data Transmission by Frequency-Division Multiplexing Using the Discrete Fourier Transform," *Communication Technology, IEEE Tran.*, Vol.19, No.5, pp. 628-634.